J Solid State Electrochem (2012) 16:2597–2603
DOI 10.1007/s10008-012-1678-7

ORIGINAL PAPER

A comparative study of activated carbon-based symmetric supercapacitors in Li_2SO_4 and KOH aqueous electrolytes

Xianzhong Sun · Xiong Zhang · Haitao Zhang · Dacheng Zhang · Yanwei Ma

Received: 22 December 2011 / Revised: 28 January 2012 / Accepted: 3 February 2012 / Published online: 22 February 2012

Abstract In this work, we have prepared activated carbon (AC)-based symmetric supercapacitor (SC) using Li_2SO_4 aqueous electrolyte instead of H_2SO_4 and KOH and obtained a device with an improved cell voltage window (CVW) of 0−1.6 V from 0 to 1.0 V. The SC using KOH electrolyte is also fabricated for comparison. The electrochemical characteristics of SCs such as cyclic voltammetry (CV), galvanostatic charge–discharge, electrochemical impedance spectroscopy (EIS) and cycle stability are investigated systematically. The possible redox reactions of electrodes that occurred in Li_2SO_4 and KOH electrolytes that restrict the CVWs are discussed. The results indicate that in the case of Li_2SO_4, the AC electrode can deliver a specific capacitance of 210 Fg^{-1} at a current density of 0.1 Ag^{-1}, and the energy density of capacitor can be as high as 16.9 Wh kg^{-1} at 200 Wkg^{-1} (based on the total mass of active electrode materials), 80% higher than that in the case of KOH.

Keywords Supercapacitors · Activated carbon · Aqueous electrolyte · Lithium sulfate

Introduction

Supercapacitors (SCs), also called electrochemical capacitors, are energy storage devices which possess higher energy density than conventional electrostatic capacitors and higher power density than secondary batteries. They can be used as primary or auxiliary power sources in renewable energy power generation/energy storage systems, electric vehicles (EVs), hybrid electric vehicles (HEVs), aerospace fields, and other heavy duty applications [1–3]. Up to now, many efforts have been devoted to improve the energy density of SCs. According to the formula, $E=1/2CU^2$, the energy density, E, is proportional to the specific capacitance, C, and the square of the working voltage, U, which indicates that the energy density can be improved by two means: (i) employing electrode materials with higher specific capacitance, e.g., high performance carbon materials [4–7], transition metal oxides [8–10] and conductive polymers [11] and (ii) fabricating SCs with high operating voltage, e.g., the symmetric SCs using nonaqueous electrolytes substituting for H_2SO_4 and KOH due to the low voltage limits of water decomposition (ca. 1.23 V) [12], and the hybrid SCs with electrode materials of AC/MnO_2 [13, 14], AC/MoO_3 [15, 16], AC/$Ni(OH)_2$ [17], AC/$LiMn_2O_4$ [18], WO_3/VO_x [19] and $MnFe_2O_4$/$LiMn_2O_4$ [20]. However, each solution has its advantages and disadvantages. Transition metal oxides and conducting polymers show good capacity performance and high electroactivity but the cycle stability is poor, while the organic electrolytes may bring about safety and environmental compatibility problems.

Nowadays, porous activated carbons (ACs) are extensively used as electrode materials due to their low cost, abundance and good cycling stability. However, as far as the AC materials are concerned, it is worth mentioning that the literature data on symmetric SCs with neutral aqueous electrolytes is seldom reported. From the point of view of exploring new electrode materials and new hybrid SCs, Qu et al. have studied the electrochemical behavior of AC electrode in Li_2SO_4, Na_2SO_4 and K_2SO_4 aqueous electrolytes by a

Electronic supplementary material The online version of this article (doi:10.1007/s10008-012-1678-7) contains supplementary material, which is available to authorized users.

X. Sun · X. Zhang · H. Zhang · D. Zhang · Y. Ma (✉)
Institute of Electrical Engineering, Chinese Academy of Sciences, Beijing 100190, People's Republic of China
e-mail: ywma@mail.iee.ac.cn

three-electrode system and observed a large stable potential window of 1.4 V [21]. Demarconnay et al. have observed, for the first time, that the symmetric carbon/carbon SC in neutral Na_2SO_4 aqueous electrolyte has a stable cell voltage window (CVW) as high as 1.6 V and a capacity retention of 88.9% even after 10^4 galvanostatic charge–discharge cycles [22]. Nevertheless, the solubility of Na_2SO_4 in water decreases dramatically with temperature in the vicinity of the freezing point of pure water, with the solubility values of 45.3 and 4.9 g (ca. 3.2 and 0.3 mol l^{-1}) at 60 and 0 °C, respectively, which limits its application at low temperature conditions. In contrast, Li_2SO_4 has more stable solubility in water, with the solubility values of 31.4 and 36.1 g (ca. 3.1 and 3.4 mol l^{-1}) at 60 and 0 °C, respectively (see the Electronic supplementary material, Fig. S1). Therefore, Li_2SO_4 electrolyte may have higher low temperature conductivity and more excellent rate capability due to its high concentration. While this paper was being prepared, it was noticed that Yang et al. newly reported the SC using the hydrated graphene film electrode in Li_2SO_4 electrolyte and obtained a high specific capacitance of 138 F g^{-1} even at the current density of 100 A g^{-1} [23].

In the present paper, we present a comprehensive investigation on the AC-based symmetric SC using a Li_2SO_4 aqueous electrolyte. The SC with an aqueous KOH electrolyte is also studied for comparison. Our results show that the SC using Li_2SO_4 electrolyte can deliver high energy density of 16.9 Wh kg^{-1} at 200 Wkg^{-1}, with an improvement of 80% in energy density compared with the case of KOH.

Experimental

Capacitor-grade AC with a specific surface area of about 2,500 m^2 g^{-1} was purchased from Carbosino Co., Ltd. (Shanghai, China) and used without any further treatment. Poly(tetrafluoroethylene) solution (PTFE, 60 wt.%, Aldrich) was adopted as binder and isopropanol solvent as dispersant. Stainless steel (SS) mesh served as a current collector in Li_2SO_4 electrolyte and nickel mesh in KOH. The AC and acetylene black powders were mixed uniformly with PTFE in a weight ratio of 70:20:10 and pressed onto current collectors to obtain electrodes. The symmetric SC was then assembled in a sandwich-type two-electrode cell (Ø16 mm button cell) using the AC electrodes separated by a polypropylene (PP) membrane. The three-electrode cell was equipped with a working electrode (AC electrode), a counter electrode (Pt plate) and a reference electrode (saturated calomel electrode, SCE, in Li_2SO_4 electrolyte; or Hg/HgO electrode in KOH electrolyte). A special two-electrode cell was adopted, which was a modification of the three-electrode cell with an AC counter electrode instead of Pt. All reported potential values were expressed versus the normal hydrogen electrode (NHE).

The electrochemical performances were characterized by cyclic voltammetry (CV), electrochemical impedance spectroscopy (EIS) and galvanostatic charge–discharge measurements using an Autolab PGSTAT302N electrochemistry station. The cycling performances were recorded on an Arbin MSTAT 4 system at a current density of 1 A g^{-1}. The carbon species on the surface of electrodes were studied by x-ray photoelectron spectroscopy (XPS) measurements on a PHI-5300 spectrometer at 1.4×10^{-8} T using Al K_α radiation.

Results and discussion

The CVs were used to evaluate the applicable CVW of the SC using Li_2SO_4 electrolyte at a sweep rate of 5 mV s^{-1}, as shown in Fig. 1a. It can be seen that the CV profiles are symmetric rectangular in shape, implying the ideal capacitive behaviors of the capacitors. Meanwhile, the curves show no obvious peaks, indicating that the SC is charged and discharged at a pseudoconstant rate over the entire voltammetric cycles [24]. As the CVW rises to 0−1.8 V, rapid increase in the positive current at higher voltage is observed, which is related to the redox reactions occurring on the positive and/or negative electrodes. Accordingly, the galvanostatic charge–discharge behaviors of SC using Li_2SO_4 were depicted in Fig. 1b. The voltages of charge–discharge curves are linearly proportional to the charge/discharge time at the CVW of no more than 0−1.6 V, verifying the pure electric double layer capacitive behaviors. As the charging voltage exceeds the thresholds, the distortion of the line caused by the redox reaction occurs. In the case of SC using KOH, the CVs and galvanostatic charge–discharge curves are similar to that of SC using Li_2SO_4, but the stable CVW is only 0−1.0 V (Fig. 1c, d).

In order to investigate the reason why the SC using Li_2SO_4 can work at such a broad voltage window, we monitored both the cell voltages and the electrode potentials simultaneously during the galvanostatic charging process employing the special two-electrode cells, as shown in Fig. 2. The CV curves of electrodes within operation potential windows corresponding to the CVWs are illustrated in Fig. 3. The potential versus voltage curves of capacitor using Li_2SO_4 show that the potentials of positive and negative electrodes are nearly linearly proportional to the cell voltages. As the CVW is larger than 0−1.8 V, a plateau potential of 1.05 V versus NHE at the positive electrode appears. On the other hand, the anodic current increases drastically when the cell voltage approaches the upper voltage limits of 1.8 V, 1.9 V and 2.0 V, accompanied by the emersion of a cathodic wave at ca. 0.6 V versus NHE. These

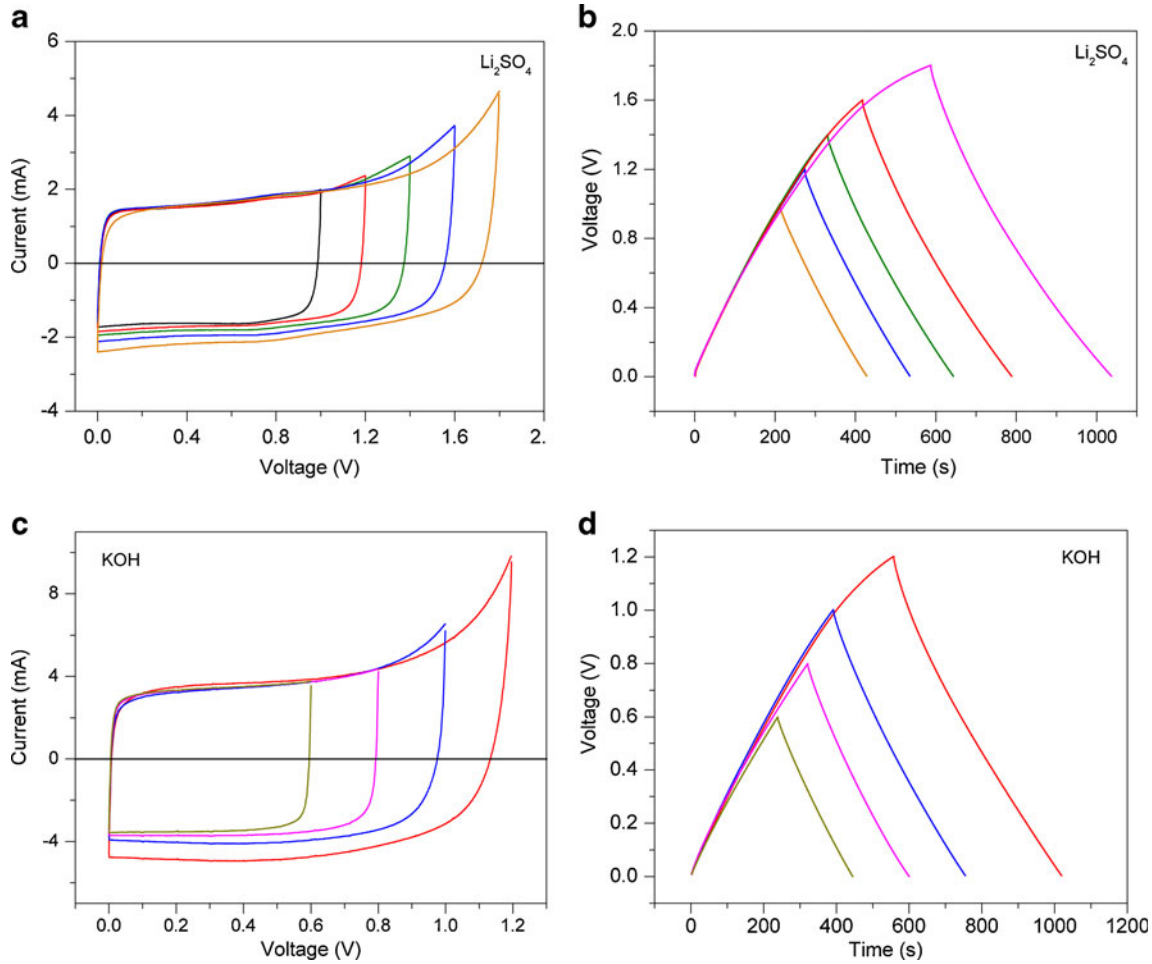

Fig. 1 **a**, **c** Cyclic voltammograms of supercapacitors at the scan rate of 5 mV s^{-1} with 1 mol l^{-1} Li_2SO_4 and 6 mol l^{-1} KOH aqueous electrolytes, respectively. **b**, **d** Galvanostatic charge–discharge curves of supercapacitors at the current density of 0.2 A g^{-1}. The cell voltate windows are: **a**, **b** 0−1.0 V, 0−1.2 V, 0−1.4 V, 0−1.6 V and 0−1.8 V and **c**, **d** 0−0.6 V, 0−0.8 V, 0−1.0 V and 0−1.2 V

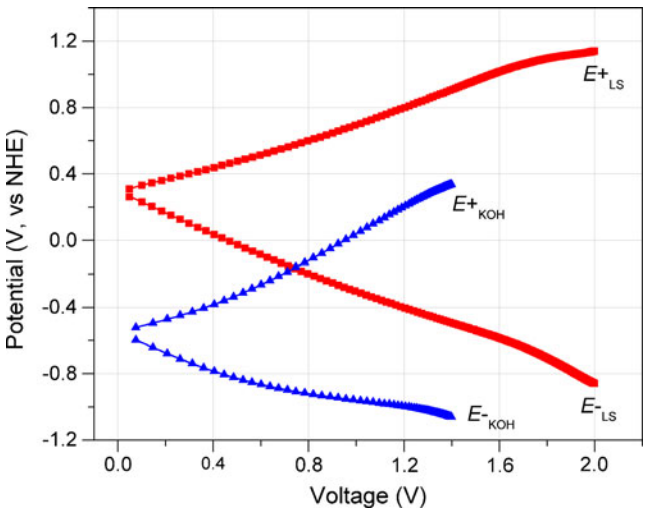

Fig. 2 Potentials of positive and negative electrodes during the charge process of a two-electrode cell (equipped with a reference electrode) with varied values of cutoff voltage. The $E+_{LS}$, $E-_{LS}$, and $E+_{KOH}$, $E-_{KOH}$ denote the potential of positive and negative electrodes in Li_2SO_4 and KOH electrolytes, respectively

behaviors of the positive electrode can be attributed to the electrochemical oxidation of oxygen-containing AC and to the redox reactions between the aqueous electrolyte and the oxidized surface functional groups [25]. The possible reactions include the following [4, 26]:

$$> C - OH \leftrightarrow > C = O + H^+ + e^- \quad (1)$$

$$> C = O + e^- \leftrightarrow > C - O^- \quad (2)$$

From the potential versus voltage curves, we can observe that the potential of the negative electrode decreases rapidly as the CVW surpasses 0−1.8 V; meanwhile, the cathodic current increases greatly. According to Béguin's group's work [22, 27], it can be related to the water reduction and hydrogen chemisorption in AC. In the neutral aqueous electrolyte, water is decomposed into atomic hydrogen and hydroxyl ion after electron transfer according to the following reaction [27]:

$$H_2O + e^- \rightarrow H + OH^- \quad (3)$$

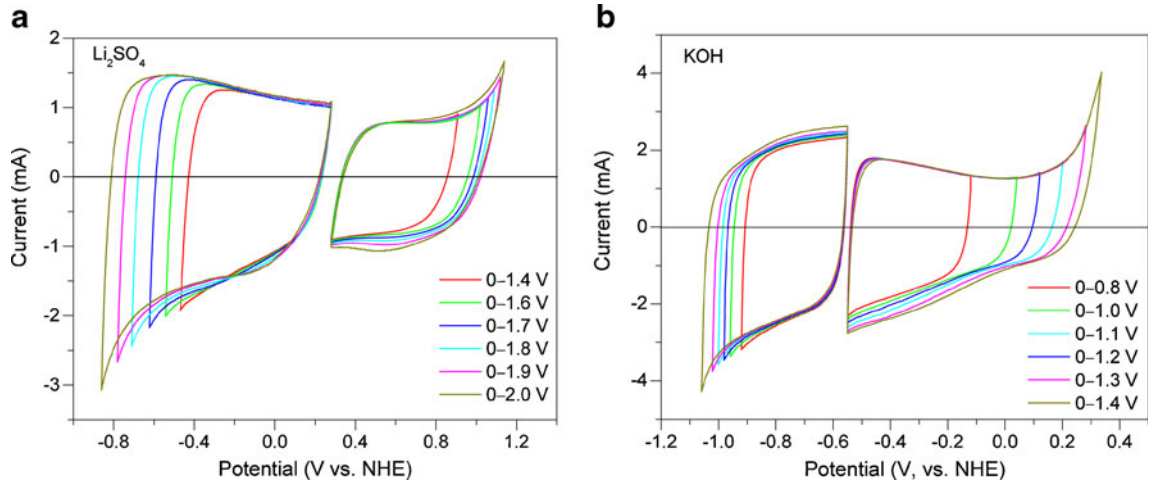

Fig. 3 Three-electrode cyclic voltammograms of positive and negative electrodes within operation potential windows corresponding to their CVWs at the scan rate of 5 mV s^{-1}, with Li_2SO_4 and KOH aqueous electrolytes, respectively

The nascent atomic hydrogen can adsorb onto the surface of AC, which is depicted as [27]:

$$H + C \rightarrow CH_{ad} \quad (4)$$

Then, the subsequent anodic current hump at ca. −0.55 V versus NHE can be ascribed to the electrooxidation of weakly adsorbed hydrogen. In the case of KOH, the obvious potential plateau of electrode has not been found from Fig. 2. Instead, the anomalous increase of anodic current corresponding to the oxygen evolution is observed as the CVW and the potential are larger than 0−1.2 V and 0.20 V versus NHE, respectively (Fig. 3b). In the strong basic solution, the oxidation process can be described as follows:

$$2\,OH \rightarrow O + H_2O + e^- \quad (5)$$

Additionally, from the CVs of electrode in Li_2SO_4 (Fig. 3a), we can find that the capacitance of the positive electrode is relatively much smaller than that of the negative electrode, which can be ascribed to the high diffusion resistance of the large hydrated anion $[SO_4{\cdot}(H_2O)_n]^{2-}$ (n=6, 12) [28] into the micropores of AC under the internal electric fields.

Electrochemical impedance spectra of the SCs using Li_2SO_4 and KOH are shown in Fig. 4, with a frequency range of 100 kHz to 0.01 Hz. The two Nyquist plots are similar in shape, namely, one semicircle at high frequency range, a straight line with a slope of close to 45° at high middle frequency region and a nearly vertical line at low frequency range. The intercept of the curve with the real impedance axis at high frequency gives the equivalent series resistance (ESR), which includes the resistance of electrolyte, the intrinsic resistance of ACs, the contact resistance between the AC and the acetylene black particles, and the contact resistance between the electrode films and the current collectors [29]. Generally, the high frequency semicircle does not exist on the impedance curve in the Nyquist plot for the ideal electric double-layered capacitor (EDLC). The origin of the high frequency semicircle is not clear yet, and the two possible causes are: (i) the porous structures of AC electrode with complex network of distributed capacitative and resistive elements and (ii) the kinetic leakage processes arising from interfacial redox reactions of impurities and surface functionalities of carbons [30]. The inclined 45° line at the high middle frequency range is characteristic of transmission-line-like behavior, attributing to the impedance correlating to the distributed resistance/capacitance in the porous AC electrodes [31–34]. Porous AC electrodes undergo nonuniform current distribution due to inhomogeneities of ohmic solution resistance along pore channels and of the contact resistance. This brings about a continuous variation of electrical relaxation rates throughout the electrode matrix,

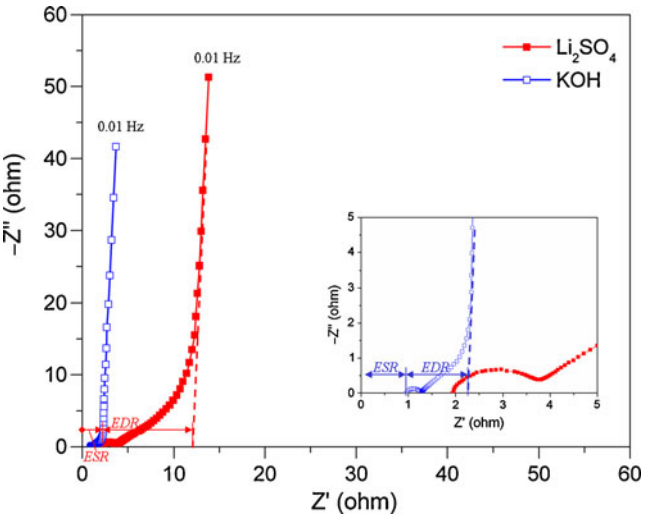

Fig. 4 Nyquist plots of capacitors filled with Li_2SO_4 and KOH aqueous electrolytes

namely, from the outer geometrical interface of the AC particles in contact with electrolyte toward pore channels and pore surfaces [30]. The resistance induced by the internal ionic solution resistance within the porous structures is called the Equivalent Distributed Resistance (EDR). The vertical line at low frequency is characteristic of capacitive behavior. The extrapolated intercept of the vertical line on the real axis gives the value of total internal resistance R = ESR + EDR [35]. From the plots, we can find that the impedance of SC using Li_2SO_4 is somewhat larger than that of the one using KOH. For the AC electrodes with identical active materials and film thickness, the increased ESR in Li_2SO_4 is mainly correlated with the electrolyte conductivity (ca. 85 and 440 mS cm^{-1} for 1 mol l^{-1} Li_2SO_4 and 6 mol l^{-1} KOH, respectively) [36, 37], and the increased EDR is rather due to the frequency-dependent resistance associated with the electrolyte penetration and the ionic dynamic dispersion within the electrode pores [21, 38].

Figure 5a, b show the galvanostatic charge–discharge curves of SCs using Li_2SO_4 and KOH at varied current densities with the CVWs of 0−1.6 V and 0−1.0 V, respectively. The linear variation of the cell voltage versus time during both charging and discharging processes is observed at all current densities. The time of charge and discharge are almost identical, which indicates the high reversibility and high coulombic efficiency of electrode materials. The specific capacitance (C_s) of the electrode can be calculated from the following equation [22, 39]:

$$C_s = 4It/M\Delta U \tag{6}$$

where I is the discharge current density, t is the discharge time within the CVW ΔU, M is the total mass of AC in both electrodes. The specific capacitance as a function of current density is shown in Fig. 5c. The specific capacitance of AC electrode in Li_2SO_4 electrolyte decreases as the current density increases, dropping from 210 Fg^{-1} at a current density of 0.1 A g^{-1} to 94 Fg^{-1} at 5 A g^{-1}. In contrast, the electrode in KOH electrolyte shows a higher capacitance, 265 Fg^{-1} at 0.25 A g^{-1}, and a better high current performance, with specific capacitance of still up to 180 Fg^{-1} at

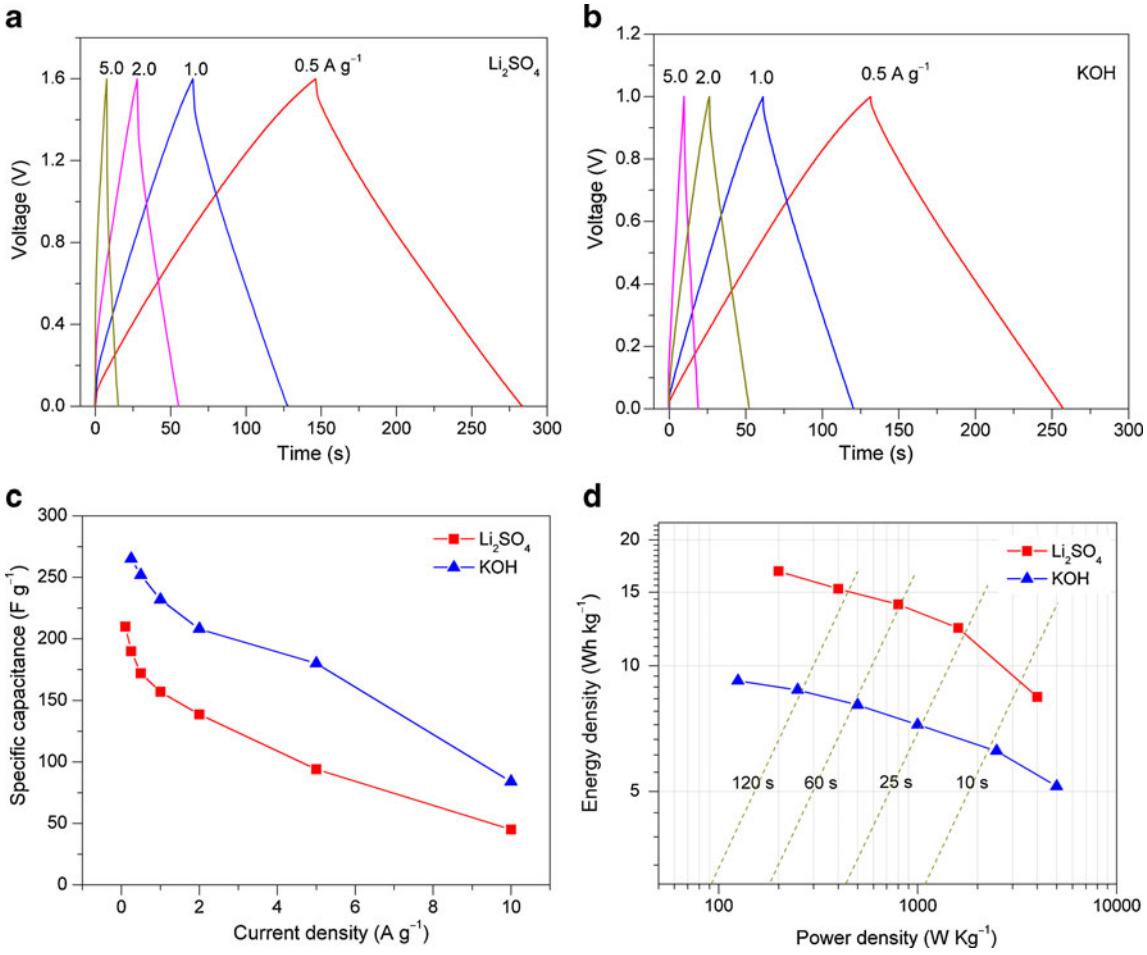

Fig. 5 **a**, **b** Galvanostatic charge–discharge curves of capacitors at current densities of 0.5, 1.0, 2.0 and 5.0 A g^{-1}. **c** Specific capacitance as a function of the current density. **d** Ragone plots of capacitors. The electrolytes are Li_2SO_4 and KOH aqueous solutions, and the CVWs are 0−1.6 V and 0−1.0 V, respectively

Table 1 Electrochemical characteristics of capacitors filled with Li_2SO_4 and KOH aqueous electrolytes

Electrolyte	Cell voltage (V)	C_s[a] (F g^{-1})	E_{max} (Wh kg^{-1})	R (Ω)	P_{max} (kW kg^{-1})
Li_2SO_4	1.6	190	16.9	12.0	6.8
KOH	1.0	265	9.2	2.2	9.5

[a] Specific capacitance and maximum energy density calculated for the mass of total active materials at the current density of 0.25 A g^{-1}

5 A g^{-1}. Taking into account the EIS analysis above, this difference of rate capability can be ascribed to the slight larger resistance of SC (e.g., ESR and EDR) in Li_2SO_4 than that in KOH.

The power density P and energy density E of SC can be derived from the galvanostatic charge–discharge data using the formula as follows [40]:

$$P = I\Delta U/2M \tag{7}$$

$$E = It\Delta U/2M \tag{8}$$

The values of P and E of SCs using Li_2SO_4 and KOH at different discharge current densities were calculated and displayed by Ragone plots in Fig. 5d. At 25 s time constant, the energy density and the power density of capacitor using Li_2SO_4 are ca. 12.3 Wh kg^{-1} and 1.6 kW g^{-1}, against that of the ones using KOH ca. 7.2 Wh kg^{-1} and 1.0 kW g^{-1}, respectively. The maximum power density, P_{max}, can be calculated from the following relationship [33]:

$$P_{max} = \frac{\Delta U^2}{4R \cdot M} \tag{9}$$

The E_{max} and P_{max} of SCs using Li_2SO_4 and KOH are 16.9 Wh kg^{-1}, 9.2 Wh kg^{-1} and 6.8 kW kg^{-1} and 9.5 kW kg^{-1}, respectively (see Table 1).

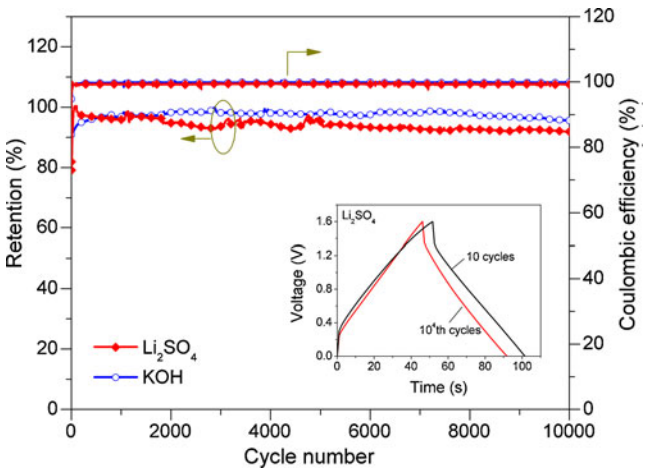

Fig. 6 Cycling stability of the capacitors with Li_2SO_4 and KOH aqueous electrolytes

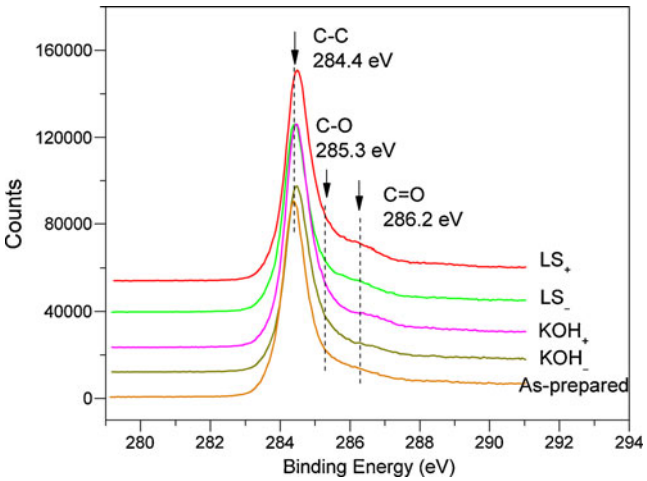

Fig. 7 The C 1s XPS spectra of the as-prepared electrode and the electrodes upon 10^4 charge–discharge cycling. The LS_+ and LS_- denotes the positive and negative electrodes in Li_2SO_4 and KOH_+ and KOH_- the ones in KOH, respectively

Figure 6 shows the galvanostatic charge–discharge cycling behavior of SC using Li_2SO_4 at a current density of 1 A g^{-1} with the CVW of 0−1.6 V. During the first 50 galvanostatic charge–discharge cycles, the discharge capacity reaches its maximum value and then decreases slowly with the cycle times. The capacitor still remains at 92.0% capacitance retention of the maximum specific capacitance after 10^4 cycles, with its coulombic efficiency of more than 99.0% at nearly entire cycles. The cycling stability is well comparable to that of the capacitor using KOH with the CVW of 0−1.0 V. After cycling, the initial distortion of charge curve at higher voltage related to the redox reactions disappears, indicating the pure electric double layer capacitance behavior. The impedance spectra of capacitor show that the impedance slightly decreased after long-term penetration (Fig. S2). The XPS survey and C 1 s spectra of the as-prepared AC electrode and the positive and negative electrodes in Li_2SO_4 and KOH upon 10^4 cycling are shown in Figs. 7 and S3. The functional groups of C–C, C–O and C = O can be observed on the surface of every electrode [41]. The C 1 s spectra ranging from 279 to 291 eV were and fitted (Fig. S4) and the relative amounts of different carbon species calculated from the deconvolution of the C 1 s XPS peaks of the electrodes are listed in Table 2. The

Table 2 Relative atomic percentages of various functional groups obtained from the deconvolution of the C 1 s peaks of the as-prepared electrode and the electrodes upon 10^4 charge–discharge cycling

at.%	As-prepared	LS_+	LS_-	KOH_+	KOH_-
C–C	80.3	76.6	78.0	78.2	78.6
C–O	13.4	15.2	14.9	15.1	15.3
C = O	6.3	8.2	7.1	6.7	6.1

atomic percentage of C–C, C–O and C = O species on the as-prepared electrode are 80.3%, 13.4% and 6.3%, respectively. After cycling, the contents of oxygen-containing groups increase slightly for both positive and negative electrodes in Li_2SO_4 and KOH. For example, in the case of Li_2SO_4, the percentage ratio of the C–O group on the surface of the positive and negative electrodes rise to 15.2% and 14.9%, respectively, near to the values of 15.1% and 15.3% in the case of KOH. The results imply that the electrochemical stability of the AC electrodes in Li_2SO_4 is comparable to that in KOH.

Conclusion

In this work, we fabricated symmetric AC-based SC devices using neutral Li_2SO_4 and basic KOH aqueous electrolytes and systematically investigated their electrochemical characteristics comparatively. We obtained stable CVWs of 0−1.6 V and 0−1.0 V and electrode-specific capacitances of 210 Fg^{-1} at a current density of 0.1 Ag^{-1} and 265 Fg^{-1} at 0.25 Ag^{-1}, in the case of Li_2SO_4 and KOH, respectively. Due to the large CVW of SC in Li_2SO_4 electrolyte, the energy density can be 16.9 Wh kg^{-1} at 200 Wkg^{-1}, 80% higher than that in KOH. After 10^4 galvanostatic charge–discharge cycling, the capacitance retention of SC in Li_2SO_4 remains at 92.0%, which is comparable to that in the case of KOH. These results indicate that the neutral Li_2SO_4 aqueous solution may be an ideal candidate electrolyte to produce cost-efficient and environment-friendly SCs.

Acknowledgments This project was supported by the Knowledge Innovation Program of the Chinese Academy of Sciences (No. KJCX2-YW-W26), the Science and Technology Project of Beijing, China (No. Z111100056011007) and the National Natural Science Foundation of China (Nos. 21001103 and 51025726).

References

1. Miller JR, Simon P (2008) Science 321:651–652
2. Zhu Y, Murali S, Stoller MD, Ganesh KJ, Cai W, Ferreira PJ, Pirkle A, Wallace RM, Cychosz KA, Thommes M, Su D, Stach EA, Ruoff RS (2011) Science 332:1537–1541
3. Simon P, Gogotsi Y (2008) Nat Mater 7:845–854
4. Xu B, Yue SF, Sui ZY, Zhang XT, Hou SS, Cao GP, Yang YS (2011) Energ Environ Sci 4:2826–2830
5. Wang XY, Liu L, Wang XY, Bai L, Wu H, Zhang XY, Yi LH, Chen QQ (2011) J Solid State Electrochem 15:643–648
6. Xing W, Huang CC, Zhuo SP, Yuan X, Wang GQ, Hulicova-Jurcakova D, Yan ZF, Lu GQ (2009) Carbon 47:1715–1722
7. Xing W, Qiao SZ, Ding RG, Li F, Lu GQ, Yan ZF, Cheng HM (2006) Carbon 44:216–224
8. Kong LB, Liu MC, Lang JW, Liu M, Luo YC, Kang L (2011) J Solid State Electrochem 15:571–577
9. Zhang X, Sun XZ, Chen Y, Zhang DC, Ma YW (2012) Mater Lett 68:336–339
10. Zhao DD, Yang Z, Kong ESW, Xu CL, Zhang YF (2011) J Solid State Electrochem 15:1235–1242
11. Zhang DC, Zhang X, Chen Y, Yu P, Wang CH, Ma YW (2011) J Power Sources 196:5990–5996
12. Zhang Q, Rong JP, Ma DS, Wei BQ (2011) Energ Environ Sci 4:2152–2159
13. Deng L, Zhu G, Wang J, Kang L, Liu Z-H, Yang Z, Wang Z (2011) J Power Sources 196:10782–10787
14. Li WC, Gao PC, Lu AH (2011) J Power Sources 196:4095–4101
15. Brezesinski T, Wang J, Tolbert SH, Dunn B (2010) Nat Mater 9:146–151
16. Tang W, Liu L, Tian S, Li L, Yue Y, Wu Y, Zhu K (2011) Chem Commun 47:10058–10060
17. Hu GX, Li CX, Gong H (2010) J Power Sources 195:6977–6981
18. Wen ZB, Tian S, Qu QT, Wu YP (2011) Prog Chem 23:589–594
19. Li JM, Chang KH, Hu CC (2010) Electrochem Commun 12:1800–1803
20. Lin YP, Wu NL (2011) J Power Sources 196:851–854
21. Qu QT, Wang B, Yang LC, Shi Y, Tian S, Wu YP (2008) Electrochem Commun 10:1652–1655
22. Demarconnay L, Raymundo-Piñero E, Béguin F (2010) Electrochem Commun 12:1275–1278
23. Yang X, He Y-S, Jiang G, Liao X-Z, Ma Z-F (2011) Electrochem Commun 13:1166–1169
24. Wang D-W, Li F, Cheng H-M (2008) J Power Sources 185:1563–1568
25. Liu XM, Wang YL, Zhan LA, Qiao WM, Liang XY, Ling LC (2011) J Solid State Electrochem 15:413–419
26. Bao QL, Bao SJ, Li CM, Qi X, Pan CX, Zang JF, Lu ZS, Li YB, Tang DY, Zhang S, Lian K (2008) J Phys Chem C 112:3612–3618
27. Béguin F, Jurewicz K, Frackowiak E (2004) Appl Phys A 78:981–987
28. Endo M, Kim YJ, Takeda T, Maeda T, Hayashi T, Koshiba K, Hara H, Dresselhaus MS (2001) J Electrochem Soc 148: A1135–A1140
29. Xu C, Du H, Li B, Kang F, Zeng Y (2009) J Electrochem Soc 156: A435–A441
30. Conway BE (1999) Electrochemical supercapacitors: scientific fundamentals and technological applications. Kluwer/Plenum, New York
31. de Levie R (1963) Electrochim Acta 8:751–780
32. Keiser H, Beccu KD, Gutjahr MA (1976) Electrochim Acta 21:539–543
33. Kotz R, Carlen M (2000) Electrochim Acta 45:2483–2498
34. Kim C-H, Pyun S-I, Shin H-C (2002) J Electrochem Soc 149:A93–A98
35. Miller JR (1995) In: Denlick FM, Tomkiewicz M, (ed) Proceedings of the Symposium on Electrochemical Capacitors: Pennington, NJ; 1995. p. 246.
36. Mosqueda HA, Crosnier O, Athouël L, Dandeville Y, Scudeller Y, Guillemet P, Schleich DM, Brousse T (2010) Electrochim Acta 55:7479–7483
37. Lewandowski A, Olejniczak A, Galinski M, Stepniak I (2010) J Power Sources 195:5814–5819
38. Portet C, Taberna PL, Simon P, Laberty-Robert C (2004) Electrochim Acta 49:905–912
39. Tian Y, Yan JW, Xue R, Yi BL (2011) J Electrochem Soc 158: A818–A821
40. Sun XZ, Zhang X, Zhang DC, Ma YW (2012) Acta Phys Chim Sin 28:367–372
41. Chen Y, Zhang X, Yu P, Ma YW (2009) Chem Commun 30:4527–4529